

Induced planet formation in stellar clusters – a parameter study of star-disk encounters

Ingo Thies^{1,2,5}, Pavel Kroupa^{1,2,3,5}, Christian Theis^{1,4}

¹*Argelander Institut für Astronomie (Sternwarte), Universität Bonn, Auf dem Hügel 71, D-53121 Bonn, Germany*

²*Institut für Theoretische Physik und Astrophysik der Universität Kiel, Leibnizstraße 15, D-24098 Kiel, Germany*

³*Heisenberg Fellow*

⁴*Institut für Astronomie der Universität Wien, Türkenschanzstraße 17, A-1180 Wien, Austria*

⁵*The Rhine Stellar Dynamical Network*

9 November 2018

ABSTRACT

We present a parameter study of the possibility of tidally triggered disk instability. Using a restricted N -body model which allows for a survey of an extended parameter space, we show that a passing dwarf star with a mass between 0.1 and 1 M_{\odot} can probably induce gravitational instabilities in the pre-planetary solar disk for prograde passages with minimum separations below 80–170 AU for isothermal or adiabatic disks. Inclined and retrograde encounters lead to similar results but require slightly closer passages. Such encounter distances are quite likely in young moderately massive star clusters (Sclally & Clarke 2001; Bonnell et al. 2001). The induced gravitational instabilities may lead to enhanced planetesimal formation in the outer regions of the protoplanetary disk, and could therefore be relevant for the existence of Uranus and Neptune, whose formation timescale of about 100 Myr (Wuchterl et al. 2000) is inconsistent with the disk lifetimes of about a few Myr according to observational data by Haisch et al. (2001). The relatively small gas/solid ratio in Uranus and Neptune can be matched if the perturbing fly-by occurred after early gas depletion of the solar system, i.e. when the solar system was older than about 5 Myr.

We also confirm earlier results by Heller (1993) that the observed 7 degree tilt of the solar equatorial plane relative to the ecliptic plane could be the consequence of such a close encounter.

Key words: stellar dynamics – methods: N-body simulations – Kuiper Belt – minor planets, asteroids – Solar system: formation – open clusters and associations: general

1 INTRODUCTION

1.1 Limits of the coagulation model

In the classical model of planet formation dust grains collide and stick together forming larger grains and clumps. These clumps also collide with each other forming progressively larger planetesimal bodies. At some point the mass of a planetesimal provides sufficient gravitation to attract surrounding particles—the accretion process begins. While the coagulation process takes several Myr for Jupiter and Saturn (Thommes, Duncan & Levison 2002), it takes at least 100 Myr for Neptune (Hollenbach et al. 2000) and probably even longer for objects in the Edgeworth-Kuiper Belt. The timescale T_{coag} of the coagulation phase is mainly determined by the density ρ of the surrounding protoplanetary dust. It further depends on the epicyclic frequency κ since the epicyclic motion is an important factor for the collision rate of planetesimals. κ is given by

$$\kappa^2 = \left(r \frac{d\Omega^2}{dr} + 4\Omega^2 \right), \quad (1)$$

where Ω is the orbital angular frequency and r the radius of the particle orbit, i.e. the distance from the central star. The dust density ρ is approximately proportional to the surface density Σ , which is expected to fit a $r^{-3/2}$ law (Weidenschilling 1977, Mayer et al. 2004). Thus for low mass disks

$$\kappa \approx \Omega \approx \Omega_{\text{Kepler}} \propto r^{-3/2}, \quad (2)$$

where Ω_{Kepler} is the Keplerian frequency. The relationship between T_{coag} and r in a gaseous disk containing fine dust with negligible gravitational interaction between the dust grains can be written as (Safronov 1969; see also Rice & Armitage 2003)

$$T_{\text{coag}} \propto \frac{1}{\Omega \Sigma} \propto r^3. \quad (3)$$

The relation may be somewhat less steep due to the smaller end masses of the outer planets and gravitational focusing for larger dust particles. This is in agreement with Pollack et al. (1996) and Kokubo & Ida (2000) who found $T_{\text{form}} \propto r^\eta$ with $\eta = 2$ and $\eta \approx 2.6$, respectively. Assuming a typical formation timescale for Jupiter's core of 3 Myr ($r_{\text{Jup}} = 5.2$ AU) this relation leads to prohibitively long formation timescales up to 600 Myr. Even the conservative r^2 law yields timescales of 40 Myr for Uranus and 100 Myr for Neptune. Thus we find good agreement of the formation-time scaling given by Eq. 3 with the more detailed investigations discussed at the beginning of this section.

Recent work by Rafikov (2004) predicts shorter formation times in the order of $\sim 10^7$ yr for the core of an ice giant at 30 AU from the Sun. Although this is only one-sixth of the conventional value, it is also near the disk lifetime discussed below and even beyond, if the accretion time of the envelope and the precursory depletion of large planetesimals (>0.1 – 1 km, Rafikov 2004) is taken into account. Goldreich et al. (2004) also predict similarly short formation timescales but require a six times higher surface density (compared to the minimum mass solar nebula, MMSN; see Weidenschilling 1977 and Hayashi 1981) in the region of Uranus and Neptune to allow them to collect most of their final mass until the end of oligarchy. This would also imply a significantly higher total disk mass.

The lifetime of the protoplanetary disk is most probably less than 10 Myr. Based on JHKL-excess observations Haisch, Lada & Lada (2001) found lifetimes less than 6 Myr before the disk material is dispersed by the stellar wind, photoevaporation and gravitational scattering by protoplanets. The masses of observed disks range from 0.003 to 0.3 M_\odot , with the bulk below 0.03 M_\odot (Natta 2004). This is comparable to the MMSN which is between 0.01 and 0.07 M_\odot . Thus, unless an unusual high disk mass or surface density profile is assumed, there is a serious problem to explain the existence of Uranus and Neptune. There have been several theoretical attempts to solve this contradiction:

(i) The coagulation and accretion process could be much faster than predicted by current models. But it seems unlikely that the models overestimate the formation times by more than an order of magnitude. Even the fast accretion scenario by Rafikov (2004) can hardly solve this inconsistency.

(ii) Protoplanetary disks could survive much longer than expected from observations like those by Haisch et al. (2001), since only the dust component of a disk can be detected by current observational methods, but no solid planetesimals. But as Uranus and Neptune mainly consist of solid material and only about 10% of gas (Wuchterl et al. 2000), this does not seem to be a satisfactory attempt either.

(iii) Uranus and Neptune may have formed much closer to the Sun in the birth region of Jupiter and Saturn and ejected from their initial orbits after reaching a certain mass (Thommes et al. 2002). With this scenario, however, it is difficult to understand the almost circular actual orbits of Neptune and Uranus.

1.2 Gravitational instabilities

Fragmentation due to gravitational instabilities (GIs) is another possible solution to this problem. The dynamical free-fall timescale of a GI in a cloud with a density excess ϱ_{exc} (relative to the ambient medium) can be estimated as

$$T_{\text{ff}} = \sqrt{\frac{3\pi}{32 G \varrho_{\text{exc}}}} \quad (4)$$

(Binney & Tremaine 1987), where G is the gravitational constant. For an over-density $\varrho_{\text{exc}} = 10^{-12}$ g cm $^{-3}$ (which would result by doubling the ambient density locally in the disk at 30 AU, the today's orbital radius of Neptune) $T_{\text{ff}} \approx 100$ yr, which is six orders of magnitude shorter than the classical formation timescale and can therefore be neglected compared to the subsequent accretion phase.

There are two major ways for the development of GIs. A very massive disk of more than 0.1 M_\odot becomes unstable to axisymmetric perturbations according to the disk stability criterion Q developed by Toomre (1964),

$$Q \equiv \frac{c_s \kappa}{\pi G \Sigma}, \quad (5)$$

where c_s is the speed of sound in the gas, κ the epicyclic frequency and Σ the surface density.

A disk can become unstable if it continues to accrete material from the protostellar cloud, so that Q becomes less than 1. For non-axisymmetric perturbations in gaseous disks, the limit is higher at $Q \simeq \sqrt{3} \approx 1.7$ (Polyachenko, Polyachenko & Strel'Nikov 1997).

Another way towards local instabilities is via tidal perturbations. With this contribution we argue that also initially stable disks can become locally unstable if an external perturbation on the surface density of the disk causes Q to fall below 1 locally, so that fragmentation only occurs in such regions. For example and as shown below, a star with mass $m = 0.5 M_\odot$ on a hyperbolic orbit with eccentricity $e = 1.5$ and pericentre distance $r_0 = 120$ AU may cause a local Toomre instability within 500 years. Such encounters are expected to occur with a realistic probability within the first 6 Myr in the Orion Nebula Cluster (Scally & Clarke 2001; Bonnell et al. 2001).

The tilt of the solar rotational axis against the normal direction of the ecliptic plane of about 7° (Eggers et al. 1997, Heller 1993) is interesting in this respect. We confirm the results presented by Heller (1993), who used smoothed particle hydrodynamics (SPH) instead of our restricted N -body calculation, that such an inclined encounter leads to the observed tilt.

In this paper we study if gravitational instabilities, as a possible originator of planet formation, can be triggered due to stellar fly-bys in a parameter survey of the stellar mass, encounter distance and eccentricity, m , r_0 and e , respectively. The aim of this survey is to identify those regions in the m - r_0 - e parameter space where growing local instabilities can be triggered. Due to the extended parameter space such a study can only be performed by fast numerical methods. Though detailed hydrodynamical calculations would be preferable for such models, they are too CPU expensive for scanning a large set of parameter space. Therefore, we applied a simple numerical ansatz based on the fast restricted N -body method as was already used by Ida et al. (2000). In the future we will use our present survey to perform hydro-

dynamical calculations for a few interesting m , r_0 and e in order to investigate the scenario of tidally triggered GIs in more detail.

In § 2 we describe our numerical model. § 3 describes the general effects of star-star encounters on circumstellar disks for an individual example. § 4 gives a plan of the parameter study and shows the results for coplanar and non-coplanar encounters. Orbits of protoplanet candidates and the tilt of the circumstellar disk due to inclined fly-bys are also described. In § 5 the results are discussed and the conclusions are presented in § 6.

1.3 Encounter probability

Tidally-induced gravitational instabilities can only be a viable mechanism if encounters are of sufficient likelihood. To estimate the encounter probability we need to consider a model of a young cluster.

Assuming a Plummer star-cluster model with given half-mass radius $R_{0.5} = R_{\text{P1}}/\sqrt{2^{2/3}-1} \approx 1.305 R_{\text{P1}}$ (R_{P1} is the Plummer-radius), mass M_{cl} and number of stars N_{cl} , we can calculate the crossing time T_{cr} from the characteristic velocity dispersion and compute the expected number of encounters n_{enc} within a given impact parameter b and therefore the mean time between encounters. This gives us a useful guide-line as to how likely the interesting encounters may be.

The relationship between b , the fly-by eccentricity e and the pericentre distance r_0 is

$$r_0 = \sqrt{\frac{e-1}{e+1}} \cdot b. \quad (6)$$

The one-dimensional characteristic velocity dispersion $\sigma_{1\text{D}}$ in the Plummer model, derived from the virial theorem, is given by

$$\sigma_{1\text{D}}^2 = \frac{\pi}{32} \frac{GM_{\text{cl}}}{R_{\text{P1}}} = \frac{\pi\sqrt{2^{2/3}-1}}{32} \frac{GM_{\text{cl}}}{R_{\text{P1}}}, \quad (7)$$

and the crossing time is

$$T_{\text{cr}} \equiv \frac{2R_{0.5}}{\sigma_{1\text{D}}} = \left(\frac{128R_{\text{P1}}^3}{\pi(2^{2/3}-1) \cdot GM_{\text{cl}}} \right). \quad (8)$$

This leads to the mean time between encounters

$$T_{\text{enc}} = \frac{T_{\text{cr}}}{n_{\text{enc}}} = \frac{T_{\text{cr}} R_{0.5}^2}{N_{\text{cl}} b^2}. \quad (9)$$

The probability P_{enc} for at least one event within the disk lifetime T_{d} can be derived from the Poisson-probability for x encounters,

$$P_{\text{enc}}(x) = \frac{\nu^x}{x!} \exp(-\nu), \quad \text{where } \nu = \frac{T_{\text{d}}}{T_{\text{enc}}}. \quad (10)$$

For at least one event,

$$P_{\text{enc}}(x \geq 1) = 1 - P_{\text{enc}}(0) = 1 - \exp\left(-\frac{T_{\text{d}}}{T_{\text{enc}}}\right). \quad (11)$$

For a young cluster with $M_{\text{cl}} = 500 M_{\odot}$, $R_{0.5} = 0.3 \text{ pc}$ and with a mean stellar mass of $0.5 M_{\odot}$ we get $10\% < P_{\text{enc}} < 32\%$ within $T_{\text{d}} = 6 \text{ Myr}$ for $60 \text{ AU} < r_0 < 200 \text{ AU}$, as shown in Fig 1. This means that such close encounters are indeed likely in young stellar clusters. The chances are even greater, up to 50%, for a

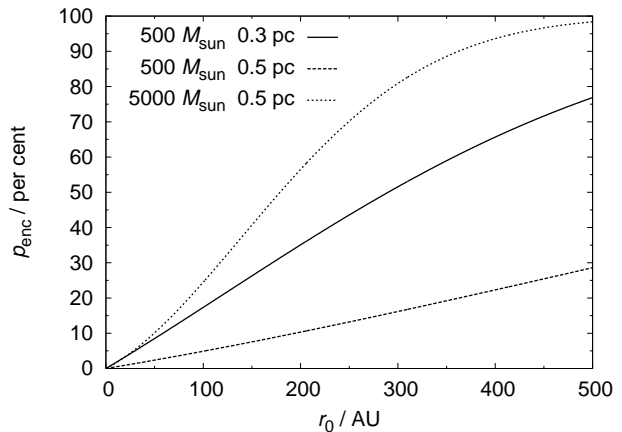


Figure 1. Probability P_{enc} of close encounters within $T_{\text{d}} = 6 \text{ Myr}$ as a function of the minimum encounter distance r_0 (Eq. 6) for three different Plummer clusters: A young open cluster of high density (solid curve), a more expanded cluster of the same mass (thick dotted curve) and a young ONC-type cluster (thin dotted curve, Kroupa et al. 2001). P_{enc} increases with increasing cluster mass M_{cl} and decreasing half-mass radius.

cluster of $5000 M_{\odot}$ and $R_{0.5} = 0.5 \text{ pc}$, similar to the Orion Nebula Cluster (ONC) (Kroupa, Aarseth & Hurley 2001). Scally & Clarke (2001) propose an encounter probability of only 4% for encounters closer than 100 AU in the ONC at its present density and age. This corresponds to a probability of 9% for $r_0 < 150 \text{ AU}$, and is still a reasonably high likelihood. We note that the probabilities for encounters in a younger and denser ONC would be accordingly higher.

2 THE MODEL

We investigate a large region of parameter space in order to study in which fraction of it tidally induced GI may be relevant. Our parameter space is defined by the distance of closest approach r_0 , the eccentricity of the relative orbit e and the mass of the perturbing star m . While an exact description of gravitational instabilities requires a 3d-stellar-hydrodynamical calculation, we apply a simpler, but numerically much faster restricted N-body approach. This ansatz is valid as long as the self-gravity of the disk, the pressure forces or the inelastic collisions between the constituents of the disk can be neglected. For example, simulations of encounters between galaxies have demonstrated the validity of this approach (Toomre & Toomre 1972). Because 3d-hydrodynamical calculations are by far too CPU intensive at the moment, such simplified dynamical modelling is the only way to scan the parameter space in detail. Of course, we cannot follow the dynamical evolution of substructures when their self-gravity becomes important or even dominant. However, we can identify regions which are prone to such instabilities.

In our computations the disk is represented by test particles on initially circular and coplanar orbits. There is no explicit interaction (self-gravity, coagulation, pressure forces) between the particles themselves and also no gravitational feedback of the disk to the Sun or the perturbing star. We assume both stars to move on hyperbolic orbits. This should

be typical for young star clusters. Our numerical method requires low computational effort. Therefore, it allows for the requested in-depth parameter study of the main orbital parameters m , e and r_0 providing an estimate of the order of magnitude of the perturbation and its probable effects on disk stability. We expect this approach to give useful insights into those regions of the encounter-parameter space where the physics will be of interest for triggered GI, because the primary mechanism driving the fluctuations in disk density within the first 500 years comes from the changes of the overall potential due to the relative orbit of the two stars.

2.1 Disk properties

In our model we suppose an initially flat disk with an outer radius $r_{\max} = 100$ AU, an inner border $r_{\min} = 3$ AU and a total mass $M_d = 0.073 M_\odot$, which is close to the Minimum Mass Solar Nebula. The surface density Σ is then given by

$$\Sigma(r) = 6300 \text{ g cm}^{-2} \cdot \left(\frac{r}{\text{AU}}\right)^{-3/2}. \quad (12)$$

For later analysis (§ 4.1) the disk is assumed to contain a dust fraction of the order of 1 per cent (Natta 2004). Thus the surface density of the dust component is approximately 1/100th of the total Σ , $\Sigma_{\text{dust}}(r) \approx 0.01\Sigma(r)$. The density profile is needed for the calculation of the local Toomre parameter Q which we use as an indicator of local gravitational instability. As shown in Eq. 5 Q depends on the speed of sound in the gas fraction of the disk, which mainly depends on the radial temperature profile. Following a recommendation by Rafikov (2004) we use

$$c_s \approx 1200 \text{ m s}^{-1} \left(\frac{r}{\text{AU}}\right)^{-0.25}. \quad (13)$$

Thus, the initial Q is approximately given by

$$Q_0 \approx 18 \left(\frac{r}{\text{AU}}\right)^{-0.25}. \quad (14)$$

The changes of Q also depend on the adopted polytropic index γ , which is given with respect to the cooling efficiency of the disk. Large cooling rates prevent tidally compressed clouds from significant heating, i.e. we have an isothermal gas, $\gamma = 1$. If the cooling is negligible the gas is compressed adiabatically. For a di-atomic gas $\gamma = 1.4$ which is a good approximation for the protoplanetary gas since it mainly consists of molecular hydrogen. Since $p \propto \rho^\gamma$ and $c_s \propto \sqrt{p/\rho}$ and $\Sigma \propto \rho$, the dependence of Q on the dynamic compression factor $\mathcal{K} (\equiv \Sigma/\Sigma_0)$ is given by

$$Q(\mathcal{K}) = Q_0 \mathcal{K}^{\frac{\gamma-3}{2\gamma}}. \quad (15)$$

The relations above are valid for gaseous disks. For disks that have already been depleted of much of their gas, e.g. either through photo-evaporation by their central star or from a nearby O star, the GIs may develop in the dust component in a similar way. The stability of a dust particle disk is then given by

$$Q_{\text{dust}} = \frac{\sigma_{\text{dust}} \kappa}{\pi G \Sigma_{\text{dust}}}, \quad (16)$$

where σ_{dust} is the velocity dispersion of the dust particles. If the disk particles and gas molecules have reached thermodynamical energy equipartition, σ_{dust} can be estimated

via the ratio of the dust particle mass m_p compared to the molecular mass μ of the gas:

$$\sigma_{\text{dust}} \sim c_s \cdot \sqrt{\frac{\mu}{m_p}}. \quad (17)$$

For micron-sized or larger particles this is negligible compared to other causes of velocity dispersion (e.g. gas turbulences which excite the dust component via gas drag). However, it is reasonable to assume the dust component to be dynamically much cooler for particles of a certain size than the gas component. The dynamical friction damps the velocity dispersion of the dust grains over a long time but the grains remain inert to short-time gas perturbations and turbulence. Barrière-Fouchet et al. (2005) show that intermediate sized dust grains (between about 1 mm and 1 m) tend so settle efficiently into a thin dust layer in the mid-plane of the disk. If we assume that the disk is already at an intermediate age, i.e. a few Myr, so that the dust has partly coagulated to at least centimetre-sized grains, a significant fraction of the dust will be concentrated in or close to the mid-plane with a low velocity dispersion. A partial depletion of the gas component will lower the particle size required for most efficient settling. Therefore we expect $Q_{\text{dust}} < Q$ and thus a higher likelihood for GIs within the dust layer once the gas has been largely depleted. However, the extension of the simulation to this case has a more qualitative than quantitative character and needs to be ascertained with hydrodynamical models. The role of the dust is discussed in more detail in § 5.

2.2 Numerical methods

Because we neglect particle-particle interactions and the disk-to-star influence, the gravitational acceleration for each test particle depends only on the position of the particle and both stars at a given time t , whereas the star-star encounter is reduced to a two-body problem. This allows to split the motion of the bodies into two parts:

- (i) The hyperbolic (or parabolic) encounter of the stars, and
- (ii) the motion of the individual particles in the time-dependent gravitational field of both stars.

For each particle the equations of motion are solved numerically. In each time step the acceleration is computed from the time-dependent stellar positions.

The time-dependent positions of the two stars are given by a (semi-)analytical calculation of the orbits. This is reduced to finding the roots of an ordinary equation. In case of parabolic orbits it can be solved analytically, whereas in the case of hyperbolic orbits a numerical solution is required. For the latter we use a Newton-Raphson method. In order to reduce the computational costs, we interpolate the orbits by a cubic spline making use of pre-tabulated orbital positions. The equation of motion of the test particles is solved by a Bulirsch-Stoer method with adaptive step size. To avoid singularities, a gravitational softening with a length of 0.001 AU has been applied.

To obtain the local Toomre parameter the surface density is measured by “probe particles” (probes), which sum-up within their probe-volume the masses assigned to the

test particles. The method is described in more detail in Appendix A.

3 SIMULATION OF INDIVIDUAL ENCOUNTERS

To demonstrate the general effects of star-star encounters we simulated the fly-by of a star with $0.5 M_{\odot}$ with $r_0 = 120$ AU pericentre distance and an eccentricity of $e = 1.5$. For comparison we reran the fly-by with a larger encounter distance of $r_0 = 150$ AU.

3.1 Initial conditions

The disk particles are initially set on circular coplanar orbits around the Sun. Depending on the kind of simulation, the particle positions are set up as a polar grid arrangement (regular distribution) or as a random distribution preserving the mean density distribution. For density evaluations the regular distribution yields less noisy numerical results. On the other hand, the calculation of the mean angular momentum (for the estimate of the tilt of the disk) requires the radial mass distribution to be as smooth as possible. Thus, we used a random reshuffling of the initial particle positions for calculating the tilt in § 4.3, employing the Mersenne Twister algorithm (Matsumoto & Nishimura 1998).

The initial distance of the Sun and the perturber is set larger than 1000 AU to prevent any significant tidal effects before the encounter. For the same reason, the simulation ends after the distance has reached at least the initial value. For higher resolution, the computed population of 250,000 particles and 1000 probes is limited to the area between 25 and 30 AU. Such a selection for increasing the spatial resolution is possible because there are no interactions between the particles. The absence of further interactions also allows for a simple scaling to other disk radii and densities, so the results can be scaled up or down for the orbits of Uranus or Pluto and the larger Kuiper belt objects. In a special run, which is described in § 5.2, we extend the simulated area to 100 AU, the known region of the Edgeworth-Kuiper-Belt. We also extended the disk area to 50 AU but reduced the particle number to 10,000 for the plots shown in Figs. 2.

3.2 Passage of a $0.5 M_{\odot}$ star at 120 AU

A close encounter of a $0.5 M_{\odot}$ star at 120 AU with $e = 1.5$ gives a good illustration of the fundamental effects of tidal perturbations on a circumstellar disk. Fig. 2 shows the overall development of the perturbed disk within 50 AU during and after an encounter at 120 AU periastron distance. Within only 400 years strong density fluctuations appear as thin tidal arms of highly compressed material. These tidal arms persist a few 10^2 years up to 10^3 years, depending on the mass and the encounter distance of the perturber. Within the spiral arms, material can be carried far outwards and even become unbound. The time-dependent surface density is shown in Fig. 3 for encounter distances of 120 AU and, for comparison, 150 AU. It can be seen that the fly-by distance has a strong influence on the magnitude of the Σ peaks; while a 120 AU fly-by causes an increase of more than

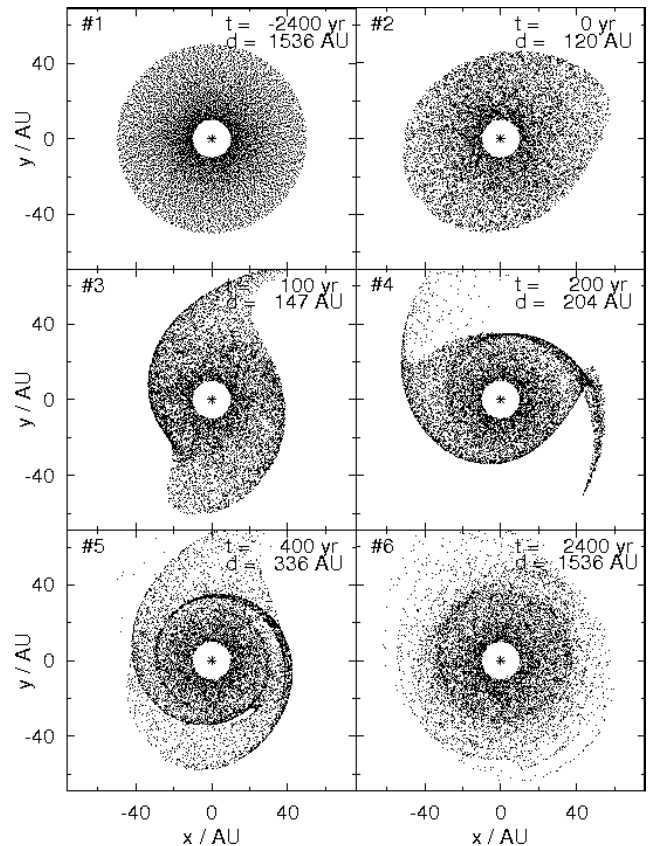


Figure 2. Disk perturbations during hyperbolic fly-by ($e = 1.5$) of a star with $0.5 M_{\odot}$ at $r_0 = 120$ AU. Only the regions within an initial radius of 50 AU are shown.

a factor of 10, the 150 AU encounter does little more than doubling Σ .

As the fly-by proceeds we follow Q in each counting volume and at each time step the minimum Q is selected. A plot of the Q_{\min} values within the computed disk area is shown in Fig. 4 for the isothermal (adiabatic index $\gamma = 1$) and the H_2/He adiabatic case ($\gamma = 1.4$). A disk with a locally isothermal equation of state and an initial $Q = 8.5$ exhibits regions with $Q < 0.8$ within less than 500 yr after a perihelion passage closer than about 120 AU, satisfying the Toomre instability criterion ($Q < 1$). For the adiabatic border case, Q locally falls to 1.2, still below the upper limit for Toomre instability $Q \approx 1.7$. According to Boss (2004), the combined convective and radiative cooling is sufficient to form clumps similarly to the isothermal case. Cooling times are of the order the orbital period even for optically thick disks and there fulfil the criterion for fragmentation investigated by Gammie (2001). Thus, an isothermal equation of state is expected to be a reasonable approximation.

4 RESULTS OF THE PARAMETER STUDY

We surveyed the parameter space (m, e, r_0) in order to find the regions where $Q < 1$ locally occurs. The parameters have been varied successively with appropriate step sizes (Tab. 1).

Here we describe the major results of our parameter study dealing with the triggering of gravitational instabilities, the masses and orbits of seed candidates for coplanar

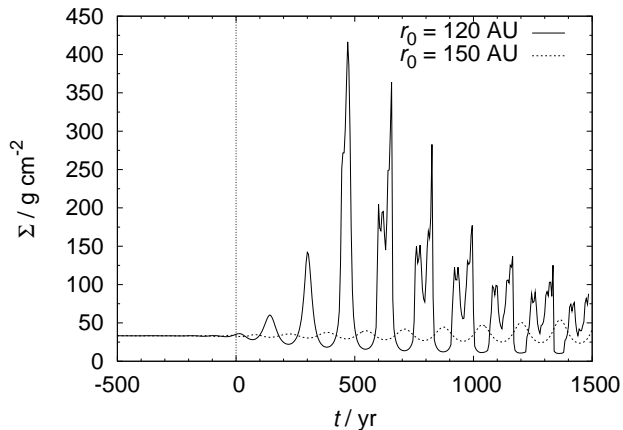


Figure 3. Surface density Σ vs time for $r_0 = 120$ and 150 AU measured in one probe at a radius of 30 AU. In the closer fly-by Σ reaches easily 10 times the initial value about 500 yr after periastron. The wider fly-by leads only to slight density variations, which illustrates the strong dependence on r_0 . The peaks in Σ are due to the density waves moving with a different velocity than the Keplerian orbital motion.

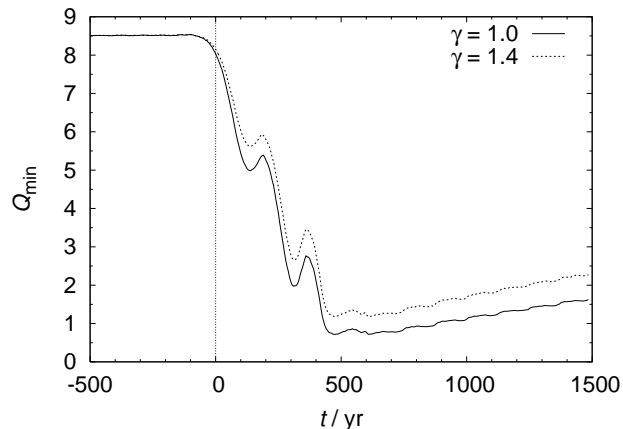


Figure 4. Minimum values of Q within the region $25 \text{ AU} \leq r \leq 30 \text{ AU}$ (initial conditions) during a 120 AU encounter of a $0.5 M_\odot$ perturber for the isothermal and the adiabatic case ($\gamma = 1.0$ and $\gamma = 1.4$, respectively). Even in the adiabatic case Q grazes the zone of Toomre instability ($Q_{\min} \approx 1.7$), whereas the more realistic isothermal case almost ensures the Toomre instability criterion ($Q_{\min} < 1$).

prograde passages, and the angular momentum tilt due to inclined passages. The possibility of triggering for inclined passages has been studied for isolated cases.

4.1 Triggered Toomre instability for prograde passages

Our parameter study for prograde coplanar passages shows that the Toomre instability criterion $Q < 1$ is locally satisfied for all stellar masses above $0.1 M_\odot$ and all eccentricities between 1 and 10 for encounter distances $r_0 \leq 80 \text{ AU}$. For perturber stars with $1 M_\odot$ and $e = 10$ we found $Q < 1$ occurrence even for fly-bys with $r_0 \leq 170 \text{ AU}$. This critical encounter radius $r_{0,\text{crit}}$, the upper limit for r_0 up to which the

	from	to	with step
m	$0.1 M_\odot$	$1.0 M_\odot$	$0.1-0.2 M_\odot$
e	1.0	10	0.5-1.0
r_0	60 AU	200 AU	5 AU

Table 1. Ranges and step sizes for the varied parameters m , e and r_0

m/M_\odot	Eccentricity e					
	1	1.5	3	5	10	50
0.1	0.77	0.71	0.61	0.53	0.44	0.26
0.3	0.73	0.68	0.58	0.50	0.41	0.25
0.5	0.69	0.64	0.55	0.48	0.39	0.24
0.7	0.67	0.62	0.53	0.46	0.38	0.23
1.0	0.63	0.58	0.50	0.44	0.36	0.21

Table 2. Coupling radius a_0 in units of r_0 , depending on the mass and orbit of the perturber

Toomre instability criterion is satisfied, depends on both the perturber mass and the encounter eccentricity in a monotonically increasing manner, as can be seen in Fig. 5. This reveals two major trends: Increasing the mass leads to an increased maximum perihelion distance $r_{0,\text{crit}}$, and also a higher eccentricity of the perturber orbit results in larger $r_{0,\text{crit}}$.

The mass dependency is simply caused by an enhanced perturbation with increasing mass. The eccentricity dependence on the other hand is less obvious. Unless the encounter velocity is extremely high or the periastron distance extremely small (i.e. close to the particle orbits) the angular velocity of the perturber is normally significantly smaller than that of the disk particles. Thus an increment of the encounter velocity for a given periastron radius yields a larger e and a smaller particle-perturber relative velocity, i.e. longer exposure time.

An important question is how much mass is included

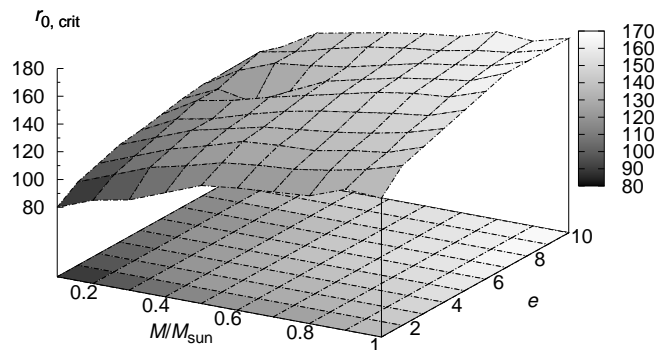


Figure 5. Upper border $r_{0,\text{crit}}$ of the regime of $Q < 1$ occurrence in the (m, e, r_0) parameter space for the isothermal equation of state. $Q < 1$ occurs for values of r_0 below the border indicated by the grid surface. Clearly visible is the increasing r_0 trend for increasing perturber mass and eccentricity. The latter trend is caused by the decreasing relative angular velocity between perturber and test particles. The key on the right indicates the r_0 -contour levels plotted in the m, e -plane.

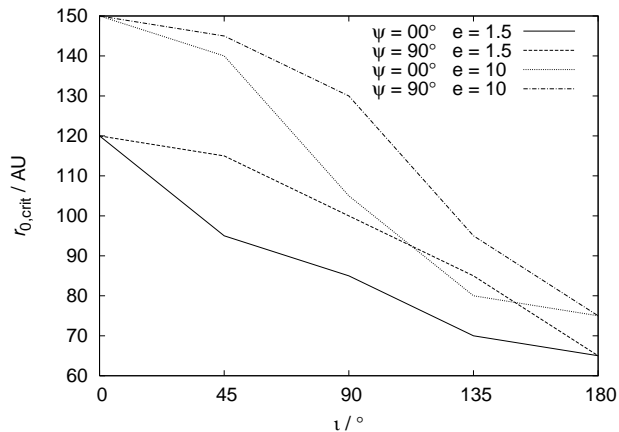


Figure 6. Critical upper pericentre distance $r_{0,\text{crit}}$ for a sample of encounters with non-zero inclination i compared to the corresponding coplanar prograde fly-by. The perturber mass is $0.5 M_{\odot}$ in all cases. Retrograde passages result in $r_{0,\text{crit}}$ about 50 % of that for zero inclination independently of the eccentricity. ψ is the angle between the pericentre and ascending node.

in a typical probe with observed $Q < 1$. A typical probe in our simulation has a radius $h = 0.1$ AU (Appendix A), but the total region of a local Toomre instability could be larger than that. In an unperturbed disk Σ has a value of about 40 g cm^{-2} or $1.5 M_{\oplus} \text{ AU}^{-2}$ at 30 AU, which results in about 0.03 Earth masses (M_{\oplus}) within h . Within a tidal arm Σ can reach 10 to 20 times this value, yielding 0.3 to $0.6 M_{\oplus}$ per probe.

Since the probe contains only a fraction of the Toomre-unstable material of the tidal arm, the total mass of the unstable region is likely to be much larger. A typical compressed arm is about 0.5 AU wide. A spherical region of 0.5 AU contains 10–20 M_{\oplus} or about one Neptune mass. If one per cent of this is dust (Natta 2004) a body of about $0.1\text{--}0.2 M_{\oplus}$ can form out of this seed. This would skip much of the coagulation time otherwise needed, and is about 100 times more massive than the most massive KBOs.

4.2 Triggered Toomre instability for retrograde and inclined passages

In a few examples we also studied the triggering effects of an inclined prograde and a retrograde passage of a $0.5 M_{\odot}$ perturber. We varied the inclinations between 45° and 180° in steps of 45° . As one would expect, the perturbation in both cases is smaller than that of a coplanar prograde passage being due to the larger distance between the perturber and that edge of the disk with the lowest angular velocity relative to the perturber. The results are summarised in Fig. 6.

For the coplanar retrograde passage (inclination = 180°), we found $r_{0,\text{crit}} = 65$ AU for $e = 1.5$ and $r_{0,\text{crit}} = 75$ AU for $e = 10$. Both are about half the $r_{0,\text{crit}}$ in the coplanar prograde case, i.e. the reduction of $r_{0,\text{crit}}$ due to inclination is apparently independent of the eccentricity. For other inclinations the decrease of $r_{0,\text{crit}}$ depends on the angle ψ between the pericentre and the ascending node, where $\psi = 90^{\circ}$ leads to significantly higher $r_{0,\text{crit}}$ than $\psi = 0$.

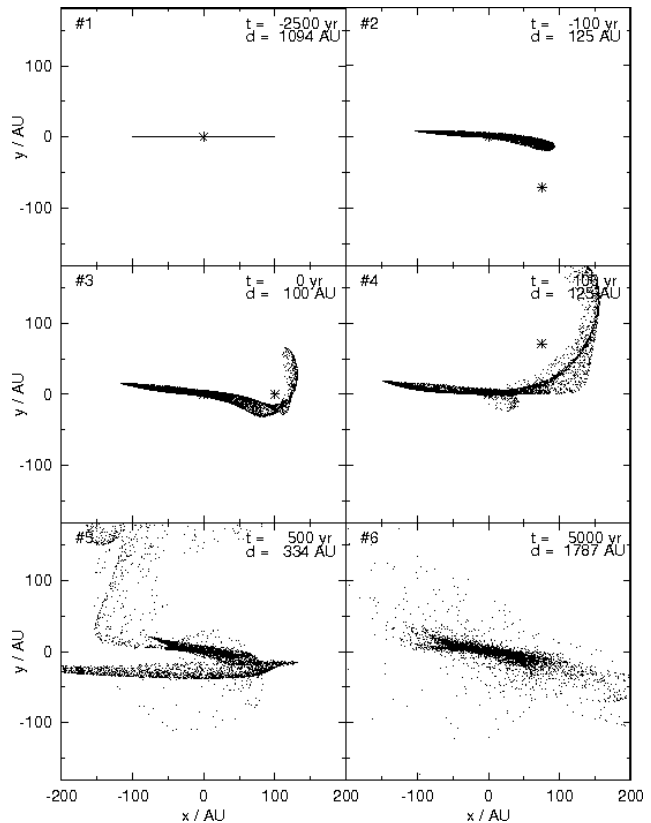


Figure 7. Parabolic fly-by of a $0.5 M_{\odot}$ star at 100 AU with 45° inclination. The angle ψ between pericentre and ascending node is 90° .

4.3 Tilt of the angular momentum vector

In inclined encounters there is the possibility for tilting the plane of the disk due to the transfer of angular momentum to the orbit of the perturber. We investigate the possible origin of the obliquity of the Sun’s rotational axis relative to the ecliptic for inclinations i between 5° and 175° and $\psi = 0$. Passages with inclination less than 90° are designated as prograde, and those beyond 90° as retrograde. In this section the radius of the model disk is set to 100 AU to measure the angular momentum change of all parts of the disk, because we expect the resulting tilt to be close to the mean tilt of the particle orbits and a global rather than a local effect. The global effects on the disk are shown in Fig. 7.

After the encounter, when the distance between the stars is large enough to prevent significant further tidal effects, the sum of the orbital angular momenta of all disk particles is calculated. The results are plotted in Fig. 8: the most remarkable feature is that the tilt has its maximum of 13° for *retrograde* passages of about 140° and $r_0 = 75$ AU, whereas the local maximum in the prograde area at 45° appears much lower for close encounters below 100 AU (6.5° for 75 AU). For less close encounters, however, the maximum tilts are essentially equal for both prograde and retrograde passages. In both cases, an encounter below about 125 AU results in a maximum tilt of more than 6° which is close to the observed solar tilt of 7° . We return to this point in § 5.3.

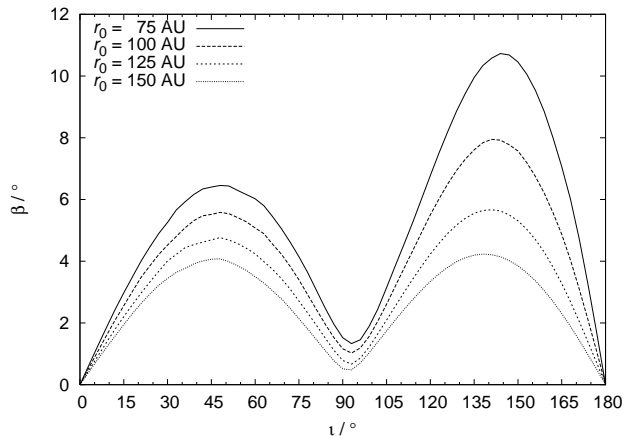


Figure 8. Tilt β of the disk after fly-by of a $0.5 M_{\odot}$ perturber as a function of inclination and closest distance. $i < 90^{\circ}$ are prograde encounters, $i > 90^{\circ}$ retrograde ones.

5 DISCUSSION

5.1 Cooling and fragmentation of disks

Based on an analytical estimate Rafikov (2005) found that the fragmentation of protoplanetary disks requires unusual high surface densities and temperatures. According to his paper a local Toomre instability does not necessarily lead to fragmentation. It is crucial that the instability can be achieved *despite* temperatures which are high enough to provide efficient radiative cooling via the Stefan-Boltzmann law. According to Rafikov (2005) the temperature T_{crit} required for efficient cooling at 10 AU ranges between 200 and more than 1000 K depending on the disk model. Only if the disk mass is a factor of 10 higher than that used by Boss (2004) is a Toomre instability possible. Because, even if the initial temperature of the condensed region is less than T_{crit} , the cloud being more unstable, the rapid increase of temperature during gravitational contraction eventually compensates the increasing pressure.

The minimum disk surface density Σ_{min} and the critical temperature T_{crit} are given by (Rafikov 2005)

$$\Sigma \geq \Sigma_{\text{min}} = \Omega^{7/5} (\pi G Q_0)^{-6/5} \left[\frac{1}{\zeta \sigma} \left(\frac{k}{\mu} \right)^4 \right]^{1/5} [f(\tau)]^{1/5} \quad (18)$$

and

$$T \geq T_{\text{crit}} = \Omega^{4/5} (\zeta \pi Q_0 G \sigma)^{-2/5} \left(\frac{k}{\mu} \right)^{3/5} [f(\tau)]^{2/5}, \quad (19)$$

where $Q_0 \approx 1$ is the upper Toomre limit for disk instability, $\zeta = 2\xi(\gamma - 1)$ is a parameter to be satisfied by the cooling time t_{cool} and the orbital frequency Ω , $\Omega t_{\text{cool}} < \xi \sim 1$. Note that our T_{crit} equals T_{min} in Rafikov (2005). σ is the Stefan-Boltzmann constant, k the Boltzmann constant, $\mu \approx 2.3$ is the molecular mass of the disk gas and

$$f(\tau) = \tau + \frac{1}{\tau}, \quad (20)$$

where τ is the optical depth which we estimate to be in the order of several tens in a compressed region. The value of τ depends on the opacity and the surface density of the particular disk region. Given the model parameters used in this

paper, an estimate of $\tau = 60$ of the compressed disk region and $\xi = 1$, conditions (18) and (19) require $\Sigma \geq 630 \text{ g cm}^{-2}$ with $T_{\text{crit}} = 330 \text{ K}$ at 30 AU. Numerical simulations suggest $\xi \approx 3$ (Gammie 2001); in that case the limits are $\Sigma_{\text{min}} = 510 \text{ g cm}^{-2}$ and $T_{\text{crit}} = 210 \text{ K}$. Assuming a tidal compression by a factor of 15 (which is a reasonable value in our simulations) the surface density condition is easily achieved in the compressed area, even with significantly lower disk masses than proposed by Boss (2004) or Mayer et al. (2004). The assumed optical thickness in these cases corresponds to a mean opacity $\omega = \tau/\Sigma \approx 0.1 \text{ cm}^2 \text{ g}^{-1}$ of the disk material, which is a reasonable value for condensed regions in protoplanetary disks (Podolak 2004; Pollack et al. 1985, for centimetre-sized dust grains).

Another problem which we do not treat in this paper is the transformation of the presumably unstable regions into (proto-)planets. In case of the formation of Neptune or Uranus this includes the question of how to get rid of a large amount of gas with respect to the dust, by this ending up with the observed high mass fraction in solid material in these planets.

In principle, the following scenarios for the evolution of a gas-rich dust disk are possible:

A dust phase can partly decouple from the gas, resulting in a comparatively thin dust layer (Natta 2004; Barrière-Fouchet et al. 2005). Since the dust evolves basically pressure-free it is much more prone to gravitational instability than the gas and, hence, instabilities in the dust phase could grow faster and form denser regions than the corresponding instabilities in the dynamically hotter gas. A plausible way of increasing the global solid-to-gas ratio is as follows: Jupiter and Saturn form traditionally within a few Myr. Meanwhile the disk is partially photo-evaporated such that the dust-to-gas ratio increases significantly, at which time the fly-by-perturbation occurs. From Fig. 5 we see that gravitational instabilities can be induced for $r_{0,\text{crit}} \leq 200 \text{ AU}$, and from Fig. 1 it can be seen that the probability of such an encounter lies between 10 and 60% if the Sun was born in a cluster with a radius of $\sim 0.5 \text{ pc}$ containing $1000 \leq N \leq 10000$ low-mass stars (one encounter within $\sim 10 \text{ Myr}$). In this scenario the GIs would be induced in a dust-dominated disk (see § 2.1).

A preferential loss of gas locally might also be possible when the clumps survive sufficiently long and mass segregation by gravity brings the dust to the center of the clumps, by this shielding the dust from a later loss by photo-evaporation. Boss (2004) suggested that the clumps can survive for a few dynamical periods which might be sufficient for the required mass segregation. Moreover, mass segregation can be possibly sped-up by vortices, as Klahr & Bodenheimer (2004) show. The solid component tends to settle rapidly in the center of a vortex due to dynamical friction. Klahr & Bodenheimer (2003) describe the formation of vortices from baroclinic instabilities. However, we expect vortices to occur also in gravitational instabilities if there is an initial spin angular momentum. The contracting GI will then be spun-up by the Coriolis forces.

In a border case the gas fraction may have been lowered due to normal depletion mechanisms during disk evolution. In the case that the dust may have already settled in or near the mid-plane, the horizontal centring due to vortices will result in an extreme concentration of dust within a small

volume, thus skipping the otherwise necessary vertical contraction due to self-gravity.

We want to stress that the discussed possibilities for getting high dust mass fractions in the clumps (i.e. an initial value problem or an evolutionary process) cannot be decided on the basis of our simple simulations. A more refined multi-component treatment of dust and gas as separate phases (e.g. as done by Theis & Orlova (2004) in the case of dusty galactic disks) would allow for investigating these in detail, but this would be part of a future investigation. We do believe, however, that our found unstable regions would be excellent large-scale seeds acting as birth places of (proto-)planets.

5.2 Orbits of candidate planetesimals

On a more speculative note our simulations allow us to study the likely initial shapes of the orbits of candidate protoplanetary seeds, which are chosen here as the probes where $Q < 1$, indicating the possible formation of a planetary core. The flyby distance is 100 AU, and two cases, a coplanar and an inclined orbit ($i = 45^\circ$) are investigated. The perturbations have their greatest impact on the region beyond 30 AU, i.e. the Kuiper belt region.

The distribution of the eccentricities e and semimajor axes a is shown in Fig. 9, where from 10000 test volumes initially at radii between 20 and 100 AU only those are plotted, for which $Q < 1$ occurred at least once.

It can be seen that the orbit of the KBO *Sedna* is not far outside the bulk of candidate seeds, and well contained in a less-dense peripheral region of candidate seeds for the coplanar case. It is still close to it in an 45° encounter. Also Pluto is contained in this population, despite its resonance with Neptune, which most probably is the result of orbital evolution after the formation. Neptune, however, lies below the candidate seed population but close to a trail of low-eccentric particles. Also due to its low eccentricity Quaoar lies outside the population. The eccentricities in this plot range from 0.02 (nearly circular) to 1 (parabolic ejection) and would even exceed 1 if plotted over the perihelion distance rather than the semimajor axis. Even the recently announced large KBO 2003 UB313 fits this plot. However, its the longitude of its ascending node deviates more from those of the other shown objects. Note that, *if the present proposition is realistic, we expect our solar system to be void of KBOs below and above the region populated in Fig. 9.*

We note that Ida et al. (2000) propose that the eccentric orbits of the Kuiper-Belt objects may have formed as a result of tidal deformation of a pre-existing planetesimal disk. Our alternative notion is that the eccentric outer-solar-system objects may be a result of an encounter which lead to the formation of Uranus, Neptune and the KBOs.

5.3 Earlier SPH simulations of tilted disks

A more extensive study of the disk tilt due to stellar encounters than ours (§ 4.3) has been made by Heller (1993), who used an SPH model with disk-star and disk-perturber interaction instead of restricted N -body computation. His results are essentially the same as in our study. Minor differences due to the absence of viscosity are possible. According to

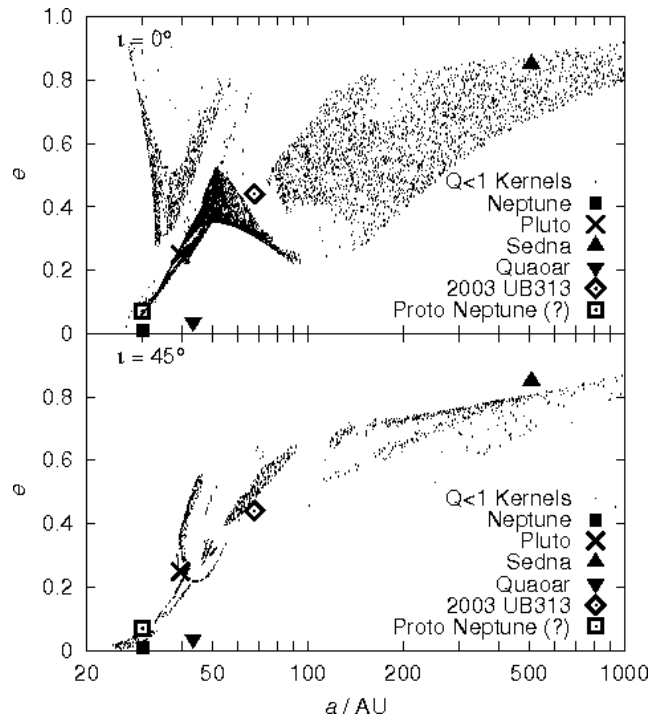


Figure 9. Distribution of semimajor axes a and eccentricities e of the $Q < 1$ probes (indicating candidate planetary seeds) after a parabolic fly-by at 100 AU with an inclination of $i = 0^\circ$ (upper panel) and $i = 45^\circ$ (lower panel). The orbits of some actual major bodies are included as well. Pluto, Sedna and 2003 UB313 are contained in or close to the main population, whereas Quaoar lies outside and Neptune below the “trail” at 25–30 AU. If the early Neptune had a slightly more eccentric orbit ($e = 0.07$) it would have fit this plot.

Heller (1993), the ability of the disk to deform, which is maximal for non-interacting test particles, enhances the resulting disk tilt. The perturbation of the perturber-star motion due to disk-star interactions also alters the results, but since the effects are small in most cases (Heller 1993), they can be neglected here. The important factor causing Heller’s results on the tilt to be somewhat larger than ours is due to his large particle removal radius of 800 AU, whereas we neglected particles with a semimajor axis larger than 150 AU.

5.4 Limits and perspectives

The restricted N -body method has its great advantage in low computational efforts. This allows us to perform a wide parameter study within an acceptable computing time, but on the other hand this also limits the accuracy of the answers.

Since we do not model self-gravity our approach is only reasonable if the mass of the disk is small compared to the solar mass, making the latter the dominant source of gravity. The same applies for the dynamical feedback on the orbit of the stars and the wobbling of the Sun (which would alter the density evolution of the disk) due to asymmetric disk perturbations.

The absence of hydrodynamical interactions limits the simulation time within which reasonable results for the density evolution can be expected. Furthermore, the effect of

cooling mechanisms as mentioned by Boss (2002) and Boss (2004) can only be approximated by adjusting the adiabatic exponent γ .

Due to these restrictions this work provides only a rough estimate of the expected magnitude of triggered instabilities. The evolution of the strong initial perturbations is determined mainly kinematically. So the results are reliable if only the immediate effects are of interest. As time proceeds the evolution will be more and more determined by hydrodynamical and other interactions within the disk. But this uncertainty mainly affects the borders of the candidate parameter subset rather than the gravitational-triggering scenario as a whole.

Despite these limitations, our study gives us an important guideline for a more tightly focussed but computationally extremely expensive hydrodynamic research.

6 CONCLUSIONS

Using a simple, but fast numerical method a parameter study has been made to test the possibility of gravitationally triggered planet formation. This scenario is supported by analytical estimates of the relatively high encounter probability in a typical young cluster (Fig. 1) as well as by the observed obliquity of the solar rotational axis being a possible consequence of an inclined fly-by.

As the main outcome of this study we summarise the following results:

(i) Prograde passages of stars with masses of 0.1–1 M_{\odot} can trigger Toomre instabilities within a 30 AU radius in a disk of 0.07 M_{\odot} if an approximately isothermal behaviour of compression is assumed. Toomre instabilities are also expected for adiabatic compression. Higher perturber masses and eccentricities increase the density perturbations and therefore allow for larger areas to become unstable.

(ii) Retrograde passages cause local $Q < 1$ for smaller r_0 (about half the value of the prograde case). Inclined passages yield $Q < 1$ for intermediately close fly-bys.

(iii) A fly-by of a 0.5 M_{\odot} star with an inclination between 30° and 60° and $r_0 \leq 100$ AU tilts the disk plane by 3°–6°. This is very similar to the observed solar obliquity.

The duration of the locally triggered gravitational instability is in the range of centuries to millennia. Therefore, if these Toomre instabilities can lead to fragmentation and enhanced core-formation they may solve the discrepancy between the short disk lifetime and the long (classical) formation times of the outer planets and maybe even the Kuiper-Belt objects (KBOs). Even if only a fraction of today's Neptune mass was assembled by triggering, this might be the required seed for the ongoing coagulation and accretion to be finished before the disk dissolves. The high solid-to-gas ratio of Uranus and Neptune may be explained in this scenario if their formation was induced by a fly-by at a solar-system age ≥ 5 Myr when the disk was depleted of gas. In this situation $Q_{\text{dust}} < Q$ such that the dust disk should be even more unstable towards GIs than suggested above. This sets possible constraints on the physical properties of the Sun's birth cluster.

Our assumed disk mass is comparable to the minimum solar nebula mass. This avoids implausible assumptions on

the disk mass as they are required for pure gravitational fragmentation of unperturbed disks.

ACKNOWLEDGEMENTS

Pavel Kroupa acknowledges support through DFG grant 1635/4-1. We thank Simon Goodwin for very useful discussions.

REFERENCES

- Barrière-Fouchet L., Gonzalez J.-F., Murray J. R., Humble R. J., Maddison S. T., 2005, A&A(in press)
- Binney J., Tremaine S., 1987, Galactic dynamics. Princeton, NJ, Princeton University Press, 1987
- Bonnell I. A., Smith K. W., Davies M. B., Horne K., 2001, MNRAS, 322, 859
- Boss A. P., 2002, ApJ, 576, 462
- Boss A. P., 2004, ApJ, 610, 456
- Eggers S., Keller H. U., Kroupa P., Markiewicz W. J., 1997, Planet. Space Sci., 45, 1099
- Gammie C. F., 2001, ApJ, 553, 174
- Goldreich P., Lithwick Y., Sari R., 2004, ApJ, 614, 497
- Haisch K. E., Lada E. A., Lada C. J., 2001, ApJ, 553, L153
- Hayashi C., 1981, Progress of Theoretical Physics Supplement, 70, 35
- Heller C. H., 1993, ApJ, 408, 337
- Hollenbach D. J., Yorke H. W., Johnstone D., 2000, Protoplastars and Planets IV, p. 401
- Ida S., Larwood J., Burkert A., 2000, ApJ, 528, 351
- Klahr H., Bodenheimer P., 2003, ApJ, 582, 869
- Klahr H., Bodenheimer P., 2004, in Revista Mexicana de Astronomia y Astrofisica Conference Series Tornados and Hurricanes in Planet Formation. pp 87–90
- Kokubo E., Ida S., 2000, Icarus, 143, 15
- Kroupa P., Aarseth S., Hurley J., 2001, MNRAS, 321, 699
- Matsumoto M., Nishimura T., 1998, ACMTMCS, 8, 3
- Mayer L., Quinn T., Wadsley J., Stadel J., 2004, ApJ, 609, 1045
- Monaghan J. J., Lattanzio J. C., 1985, A&A, 149, 135
- Natta A., 2004, in ASP Conf. Ser. 324: Debris Disks and the Formation of Planets Circumstellar Disks in Pre-Main Sequence Stars. pp 20–+
- Podolak M., 2004, in Revista Mexicana de Astronomia y Astrofisica Conference Series Dust Opacity and the Contraction of Protoplanetary Atmospheres. pp 104–107
- Pollack J. B., Hubickyj O., Bodenheimer P., Lissauer J. J., Podolak M., Greenzweig Y., 1996, Icarus, 124, 62
- Pollack J. B., McKay C. P., Christofferson B. M., 1985, Icarus, 64, 471
- Polyachenko V. L., Polyachenko E. V., Strel'Nikov A. V., 1997, Astronomy Letters, 23, 483
- Rafikov R. R., 2004, AJ, 128, 1348
- Rafikov R. R., 2005, ApJ, 621, L69
- Rice W. K. M., Armitage P. J., 2003, ApJ, 598, L55
- Safronov V. S., 1969, Evolution of the Protoplanetary Cloud and Formation of the Earth and Planets. NASA Tech. Trans., Moscow
- Scally A., Clarke C., 2001, MNRAS, 325, 449
- Theis C., Orlova N., 2004, A&A, 418, 959

- Thommes E. W., Duncan M. J., Levison H. F., 2002, *AJ*, 123, 2862
 Toomre A., 1964, *ApJ*, 139, 1217
 Toomre A., Toomre J., 1972, *ApJ*, 178, 623
 Weidenschilling S. J., 1977, *Ap&SS*, 51, 153
 Wuchterl G., Guillot T., Lissauer J. J., 2000, *Protostars and Planets IV*, p. 1081

APPENDIX A: DENSITY EVALUATION

Calculation of the local Toomre disk stability requires the evaluation of the local surface density. At first, all disk particles are weighted by an individual mass m_b which corresponds to its initial orbit radius r_b in such a way that

$$\sum_1^N m_b = M_d(r_1 \leq r \leq r_2), \quad (\text{A1})$$

where r_1 is the inner and r_2 the outer border of the simulated disk region. Since the N particles are initially positioned on a polar grid consisting of n_r rings with n_φ particles each, which results in a r^{-1} law of the surface density Σ , the mass-weighting must be proportional to $r^{-1/2}$ to fit the needed $r^{-3/2}$ law (Eq.12). Together with eqn. (A1) this leads to

$$m(r_b) = \frac{r_b^{-1/2}}{\sum_{b=1}^N r_b^{-1/2}} \cdot \frac{\sqrt{r_2} - \sqrt{r_1}}{\sqrt{r_{\max}} - \sqrt{r_{\min}}} \cdot M_d, \quad (\text{A2})$$

where r_{\min} and r_{\max} are the inner and outer radius of the *real* disk. Here we use $r_{\min} = 3$ AU and $r_{\max} = 100$ AU.

The density evaluation is achieved by simply adding the m_b within “counting-volumes” surrounding massless probe particles which move along with the disk particles on ballistic (Keplerian) orbits. Within the counting-volume the density is calculated in SPH-style using

$$\langle \varrho \rangle_W = \sum_{b=1}^N m_b W(d_b, h), \quad (\text{A3})$$

where d_b is the distance of the b -th mass-weighted test particle from the center of the probe particle. The *kernel function* W provides a smooth distance-weighting of the test particles for reduction of numerical noise. In our model the compact spline kernel from Monaghan & Lattanzio (1985) is used. The choice of the kernel radius h determines the mean number of particles n_h within the probe volume. For a random distribution, $n_h \geq 100$ is required to keep the noise low enough. A regular distribution, as we used here, shows appropriate results even for $n_h \approx 10$. For a given (average) n_h and disk population parameters r_1 , r_2 and N we get h from

$$h = \sqrt{\frac{n_h (r_1 + r_2) (r_2 - r_1)}{N}}. \quad (\text{A4})$$

Thus, typically, $h = 0.1$ AU for $r_1 = 25$ AU, $r_2 = 30$ AU and $N = 250000$.

Since we want to identify unstable regions, i.e. regions where $Q < 1$ locally, we applied about 1000 of these test volumes, which concentrate at the areas of the highest density. Their dynamic behaviour is the same as that of the disk test particles. Thus, a high spatial resolution at the areas of interest is automatically provided.